

Supplementary Information

Highly Active Quinone Sites-Enriched Carbon Nanotube Composites for Efficient Electrocatalytic Hydrogen Peroxide Generation

Yuwen Tian,^a Qianqian Wang,^a Yanyan Song,^a Jifa Yang,^a Jinzheng Liu,^a Xuejun Liu,^{*a}
and Lixue Zhang^{*a}

^aCollege of Chemistry and Chemical Engineering, State Key Laboratory of Bio-fibers and Eco-textiles, Qingdao University, Qingdao 266071, China

Experimental Section

Materials: Multi-walled carbon nanotube (MWCNT) was purchased from Shenzhen Nanotech Port Co., Ltd. sodium sulphide (Na_2S), 1,5-dichloroanthraquinone (DCAQ) and cerium sulfate ($\text{Ce}(\text{SO}_4)_2$) were purchased from Aladdin. N-methyl pyrrolidone (NMP) were purchased from Macklin. KOH (98%), HCl (35-37%) and isopropanol were purchased from SINOPHARM. Nafion ionomer (5wt%, Dupont). The deionized (DI) water used throughout all experiments was purified through a Millipore system.

Purification of CNT: The pristine MWCNTs were mixed with 3 M HCl in a 250 mL three-necked flask. After stirring at 80 °C for 12 h, the treated MWCNTs were vacuum filtered, washed with a large amount of DI water until the final pH of filtrate reached 7, and then dried at 60 °C overnight.

Synthesis of poly (anthraquinone sulfide) (PAQS)/CNT: Typically, the treated MWCNTs (80 mg) were first dispersed in 80 mL NMP. Then the mixture was sonicated for 120 min and transferred into a three-necked flask. After sodium sulfide nonahydrate (156 mg, 468 mg, 780 mg) and DCAQ (172 mg, 516 mg, 860 mg) were added into the mixture, the suspension was stirred under refluxing at 200 °C for 10 h. Finally the product was centrifuged after cooling to room temperature, washed with deionized water and acetone for several times, and then dried at 120 °C for 12 h to obtain PAQS/CNT-1, PAQS/CNT-2, PAQS/CNT-3. The pure PAQS polymer was prepared by the similar method as PAQS/CNT-1 except for the absence of CNT.

Material Characterization: FT-IR spectra were measured with KBr pellets on a Thermo Scientific Nicolet iS20 FTIR spectrometer. Thermogravimetric measurement was performed in a nitrogen stream using a Netzsch TG 209F3 apparatus with a heating rate of 5 °C min^{-1} . The morphology characterization of the materials were investigated using a field emission SEM (ZEISS Gemini 300) and TEM (FEI TalosF200x). XPS was performed on Thermo Scientific K-Alpha with Al K_α as the X-ray source.

Electrochemical Measurements: The electrochemical measurements were carried out in a three-electrode system controlled by a CHI 760E electrochemical workstation. A

graphite rod and a saturated calomel electrode (SCE) were used as the counter electrode and reference electrode, respectively. To prepare the the working electrode, 5 mg sample was dispersed in a mixture of isopropanol (960 μL) and nafion (40 μL), and sonicated for 2 h. Then, 5 μL of catalyst ink was carefully dropped onto the rotating ring-disk electrode (RRDE). After the solvent was evaporated, the working electrode was ready for electrochemical measurement and the areal loading of the electrocatalysts is 0.20 mg cm^{-2} .

The cyclic voltammetry (CV) measurements were conducted in O_2 -saturated and N_2 -saturated 0.1 M KOH+1 mM CTAB with a scan rate of 50 mV s^{-1} . LSV-RRDE tests were performed using the RRDE in O_2 -saturated and N_2 -saturated 0.1 M KOH with or whitout 1 mM CTAB solution at a potential range from 0.2 to 1.2 V (vs. RHE) with a sweep rate of 10 mV s^{-1} at 1600 rpm. The ring electrode was set at a constant potential of 1.5 V vs. RHE to detect the as-generated H_2O_2 . Long-term stability test was carried out in O_2 -saturated solution for 20 h with the disk and ring electrode potential set at 0.5 and 1.5 V vs. RHE, respectively. The H_2O_2 selectivity (H_2O_2 %) and the transferred electron number (n) were calculated based on the values of both disc and ring currents according to the following equation, where I_r is the ring current, I_d is the disk current and N is the collection efficiency.

$$\text{H}_2\text{O}_2 \% = 200 \times (I_r / N) / (I_d + I_r / N) \dots\dots\dots (1)$$

$$n = 4 \times I_d / (I_d + I_r / N) \dots\dots\dots (2)$$

Tafel slopes were calculated using the data extracted from LSV curves according to the following equation:

$$E_{\text{SCE}} = b \log(j/j_0) \dots\dots\dots (3)$$

where E_{SCE} is the potential versus SCE, b is the Tafel slope, j is the disk current density, and j_0 is the exchange current density. All potentials measured were then calibrated to reversible hydrogen electrode (RHE) using the following equation:

$$E_{\text{RHE}} = E_{\text{SCE}} + 0.241 + 0.059 \times \text{pH} \dots\dots\dots (4)$$

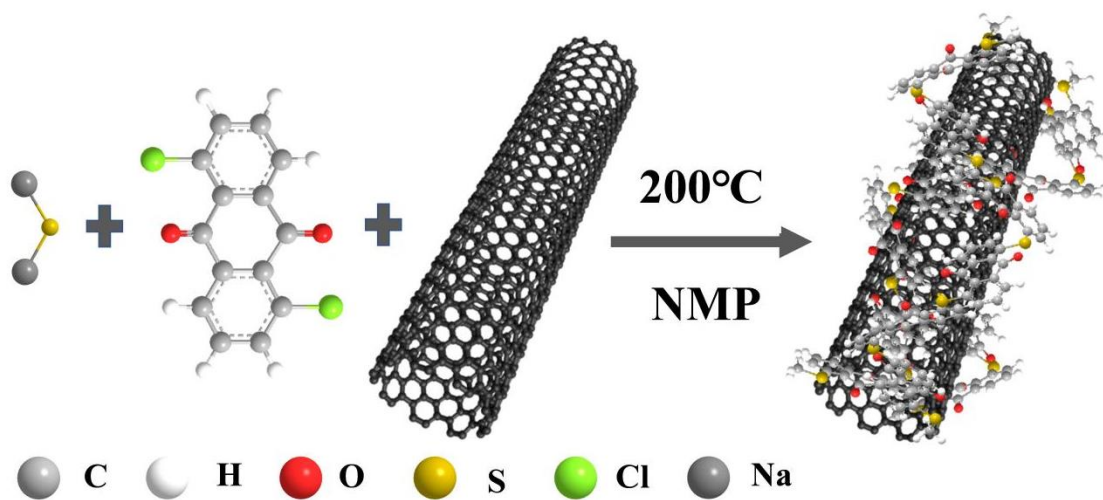


Figure S1. *In situ* polymerization process of PAQS/CNT composites.

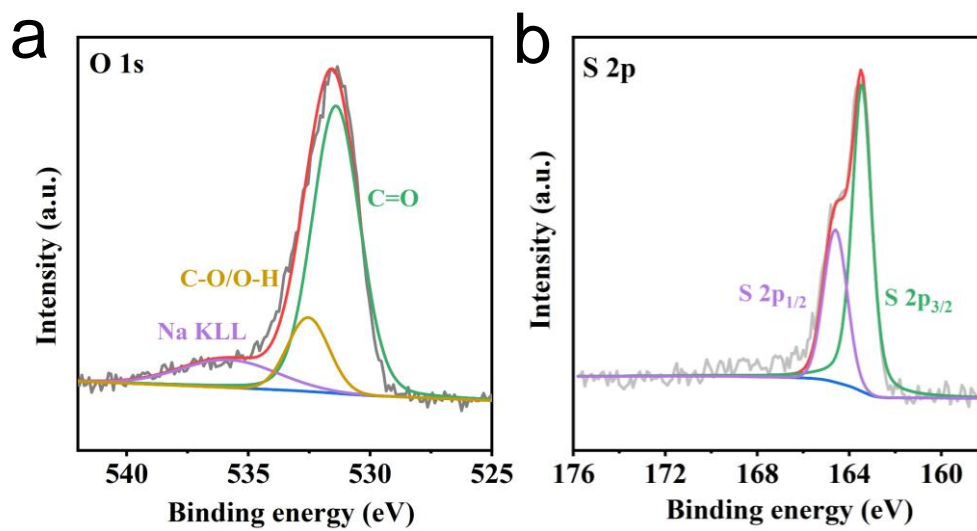


Figure S2. (a) O 1s and (b) S 2p XPS spectra of PAQS/CNT composites.

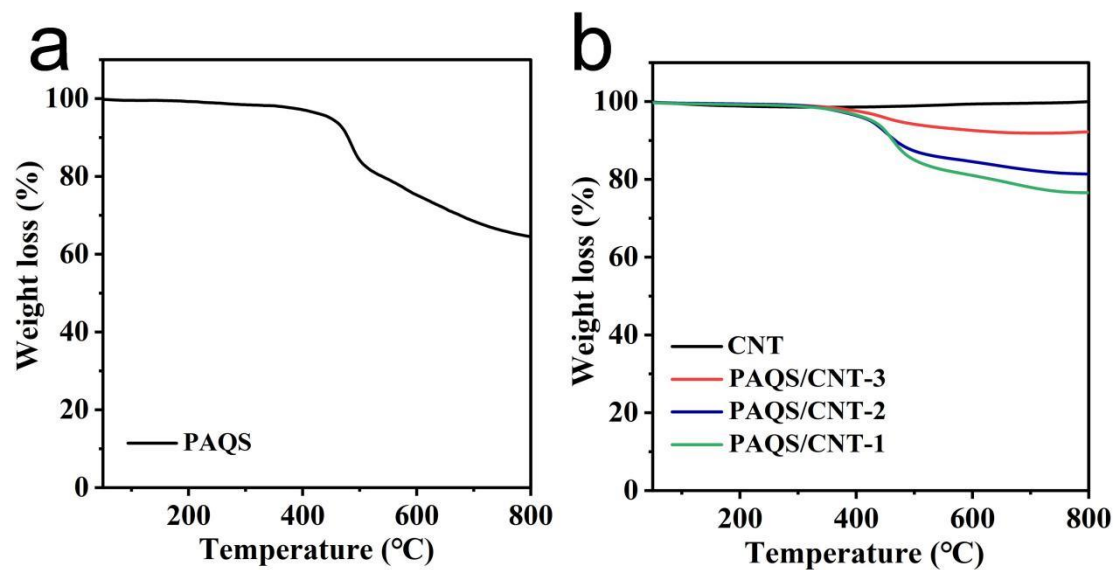


Figure S3. Thermogravimetric curves of (a) pure PAQS and (b) PAQS/CNT composites with different proportions of CNT.

From TGA curves of PAQS/CNT-1~3 it can be observed that the weight losses of different composites were measured to be 15.1%, 18.6%, and 23.4%, respectively. For the calculation of PAQS in PAQS/CNT-1~3, the weight loss of pure PAQS polymer was measured by TGA test (Fig. S3a) and the value is calculated to be 35.5%. Assuming that the weight loss of PAQS in PAQS/CNT-1~3 remained unchanged, the weight ratio PAQS in PAQS/CNT-1 is $23.4\%/35.5\%=65.9\%$, the weight ratio PAQS in PAQS/CNT-2 is $18.6\%/35.5\%=52.4\%$, and the weight ratio PAQS in PAQS/CNT-3 is $15.1\%/35.5\%=42.5\%$.

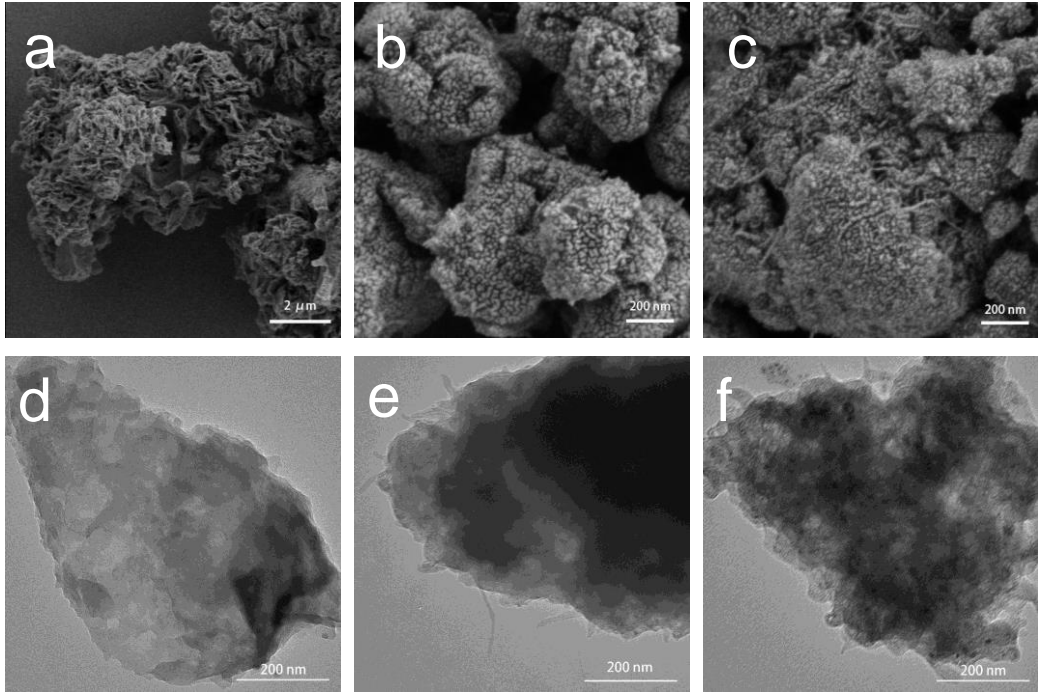


Figure S4. SEM images of (a) PAQS, (b) PAQS/CNT-1, (c) PAQS/CNT-2. TEM images of (d) PAQS, (e) PAQS/CNT-1, (f) PAQS/CNT-2.

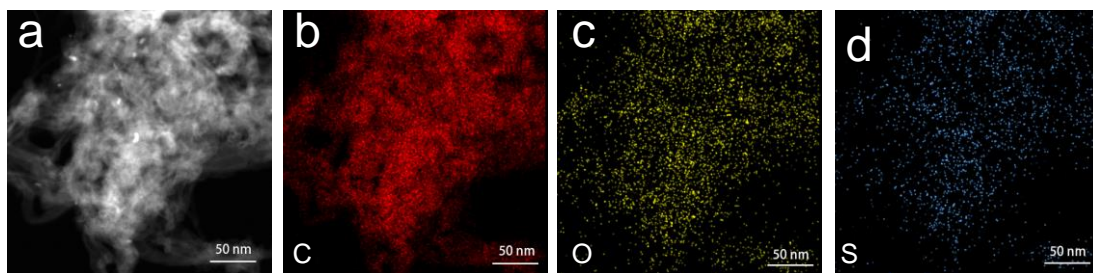


Figure S5. Elemental mappings of PAQS/CNT-3.

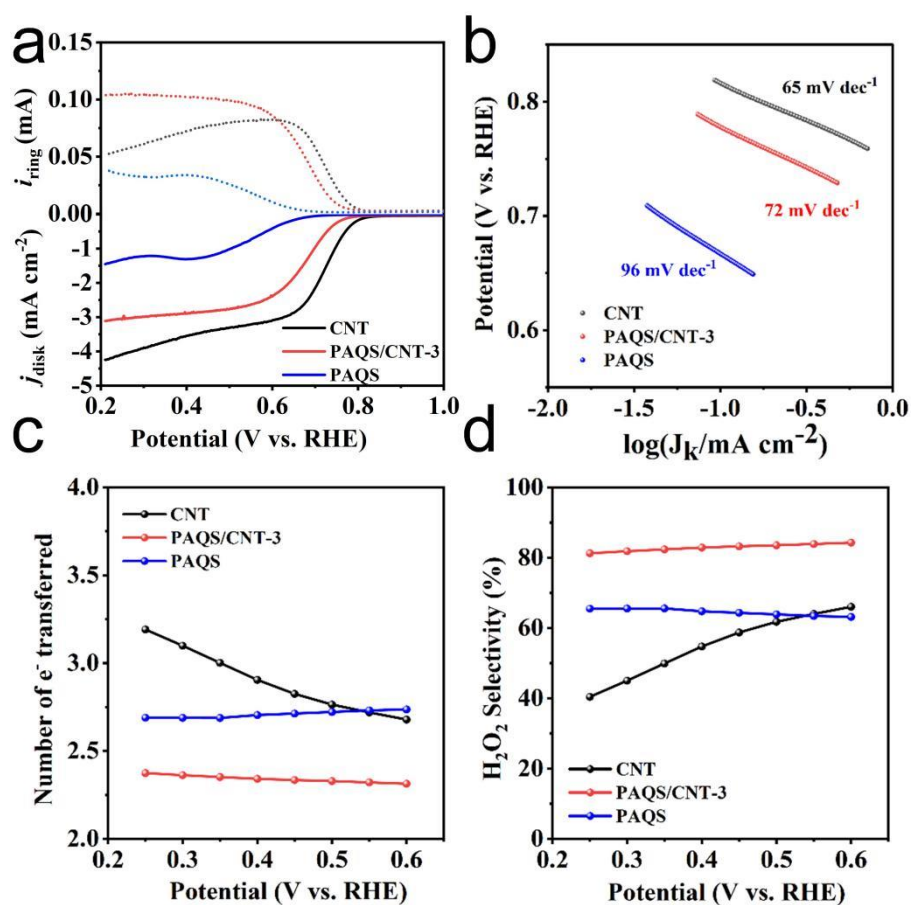


Figure S6. (a) RRDE voltammograms of PAQS, CNT and PAQS/CNT-3 in O₂-saturated 0.1 M KOH at 10 mV s⁻¹. (b) Tafel plots. (c) Number of transferred electrons. (d) Calculated selectivity.

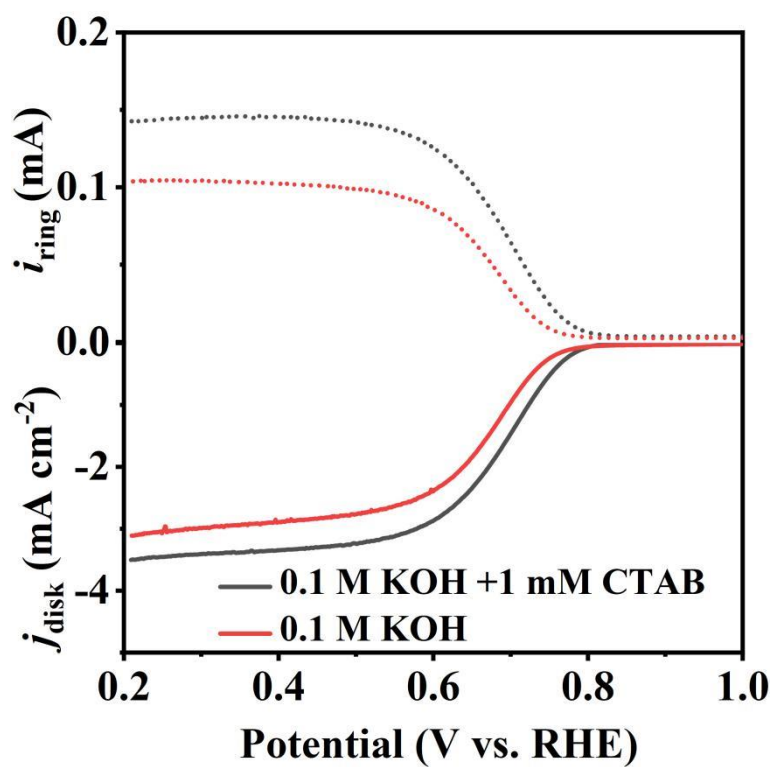


Figure S7. LSV-RRDE profiles of PAQS/CNT-3 in O₂-saturated 0.1 M KOH solution with or without CTAB.

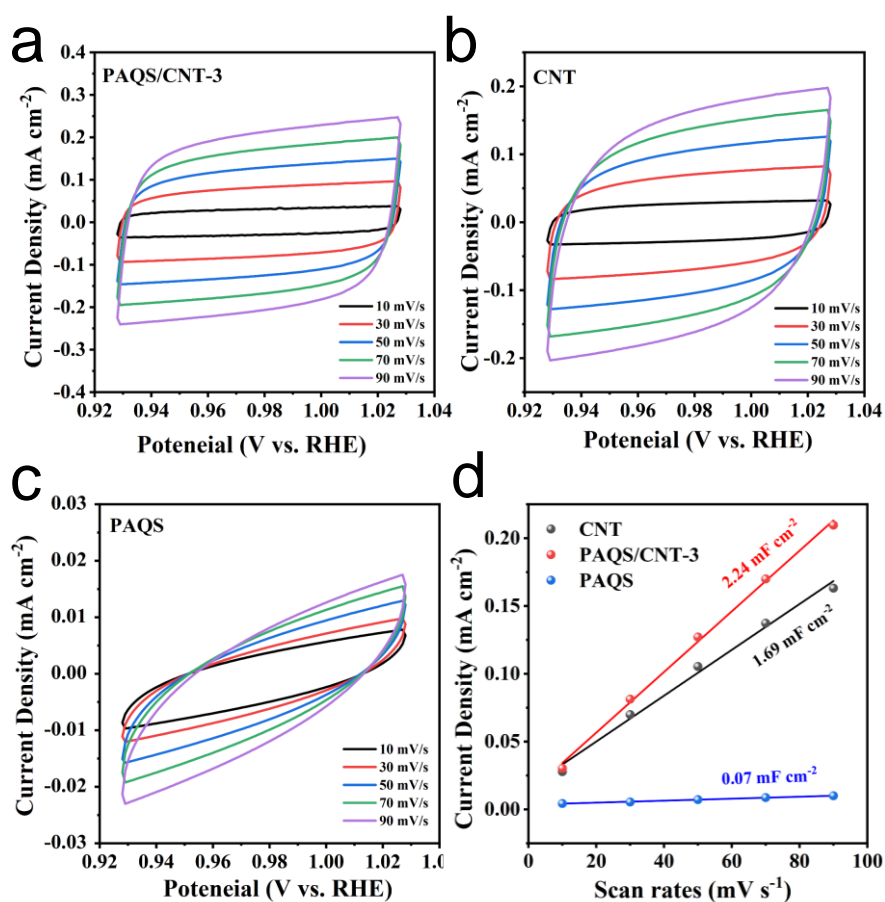


Figure S8. Determination of the C_{dl} . Cyclic voltammety curves recorded at 10, 30, 50, 70, 90 mV s^{-1} of (a) PAQS/CNT-3, (b) CNT, (c) PAQS. (d) Current density at 0.98 V (vs RHE) as a function of scan rate along with the linear fitting curves of (a) PAQS/CNT-3, (b) CNT, (c) PAQS are shown.

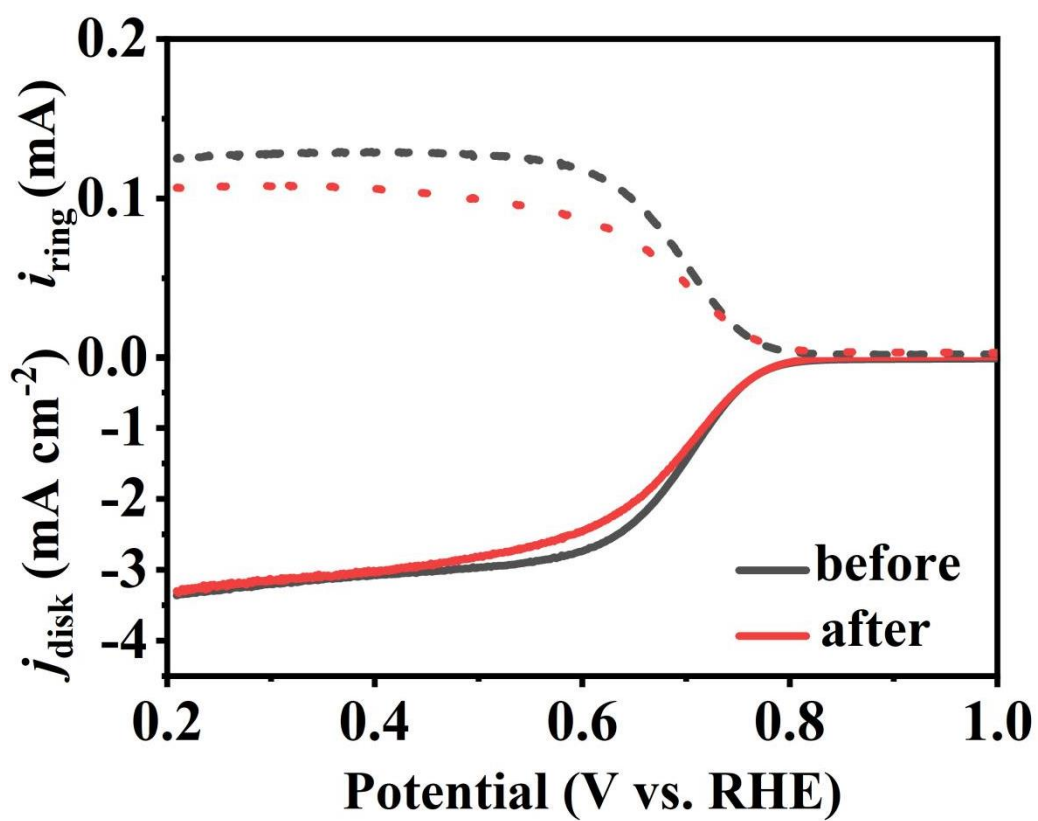


Figure S9. Comparison of RRDE voltammograms of PAQS/CNT-3 before and after stability test.

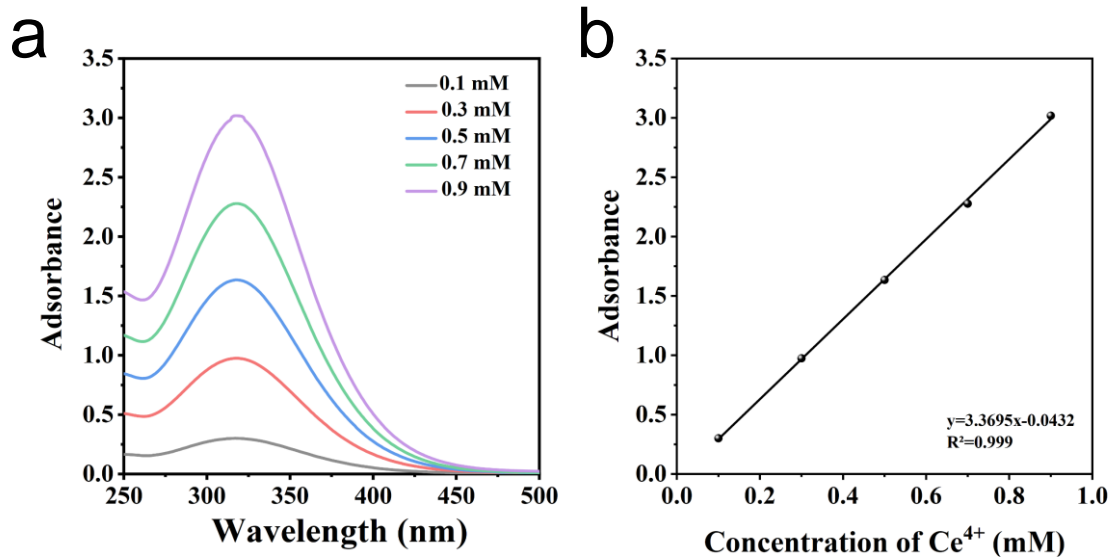


Figure S10. (a) UV-vis spectra of Ce^{4+} solution with various concentrations, and (b) corresponding standard curve.

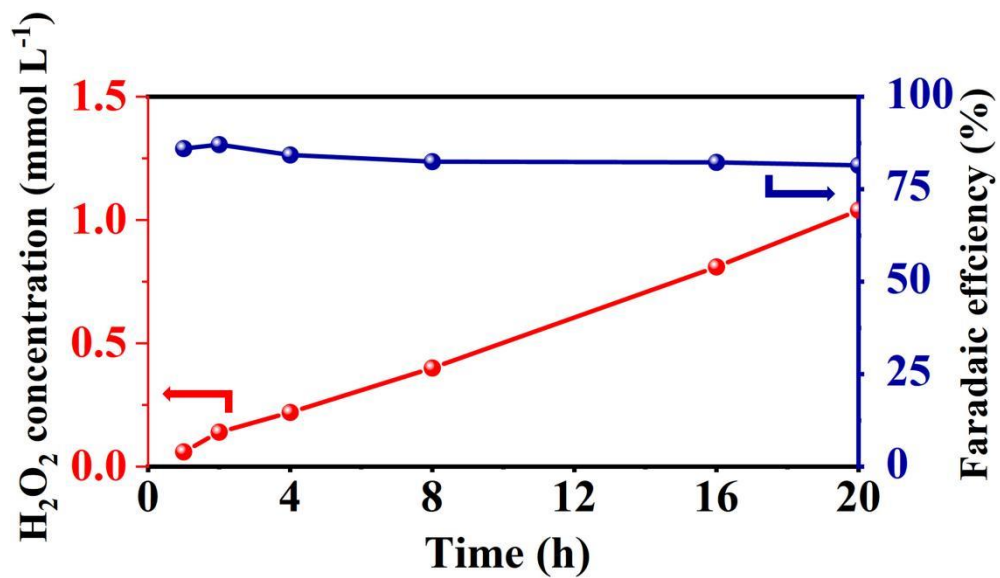


Figure S11. Accumulation amount and faraday efficiency of H₂O₂ during 20-h test

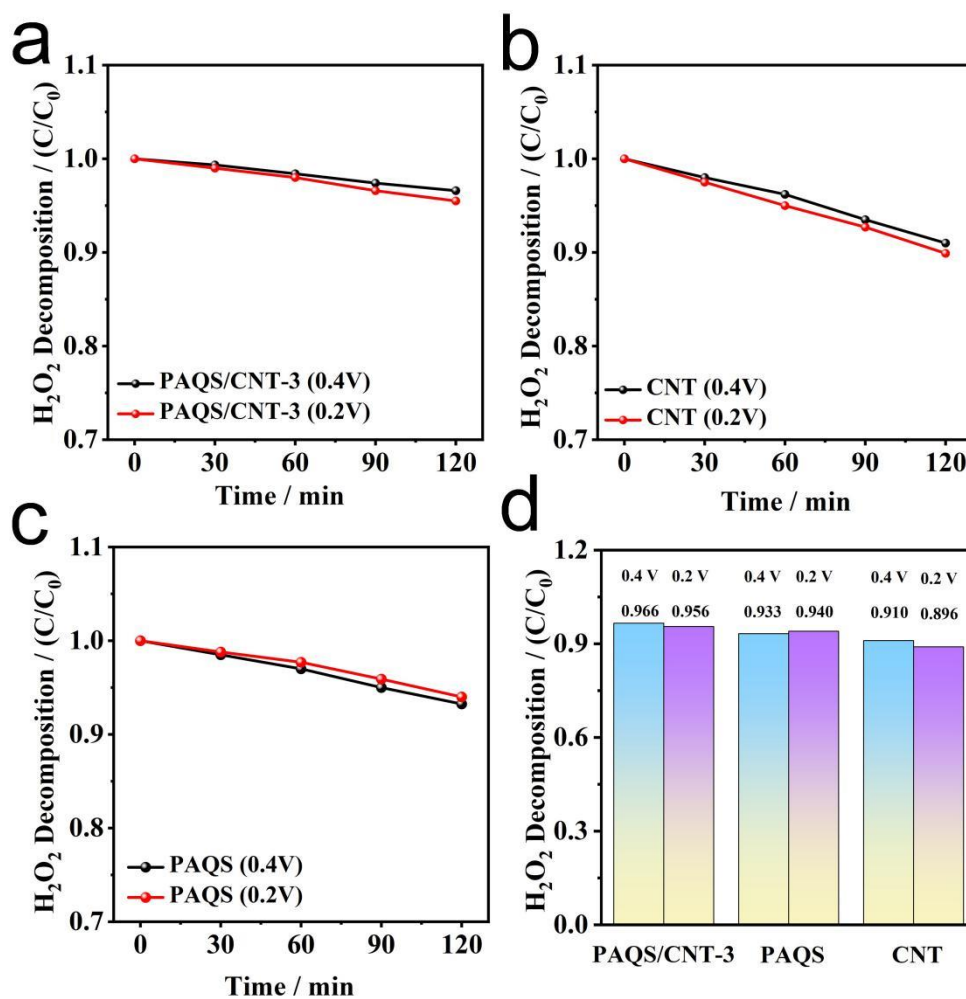


Figure S12. Electrochemical decomposition of H_2O_2 for PAQS/CNT-3, PAQS, and CNT at different voltage in 0.1 M KOH solution containing 0.5 mM H_2O_2 .

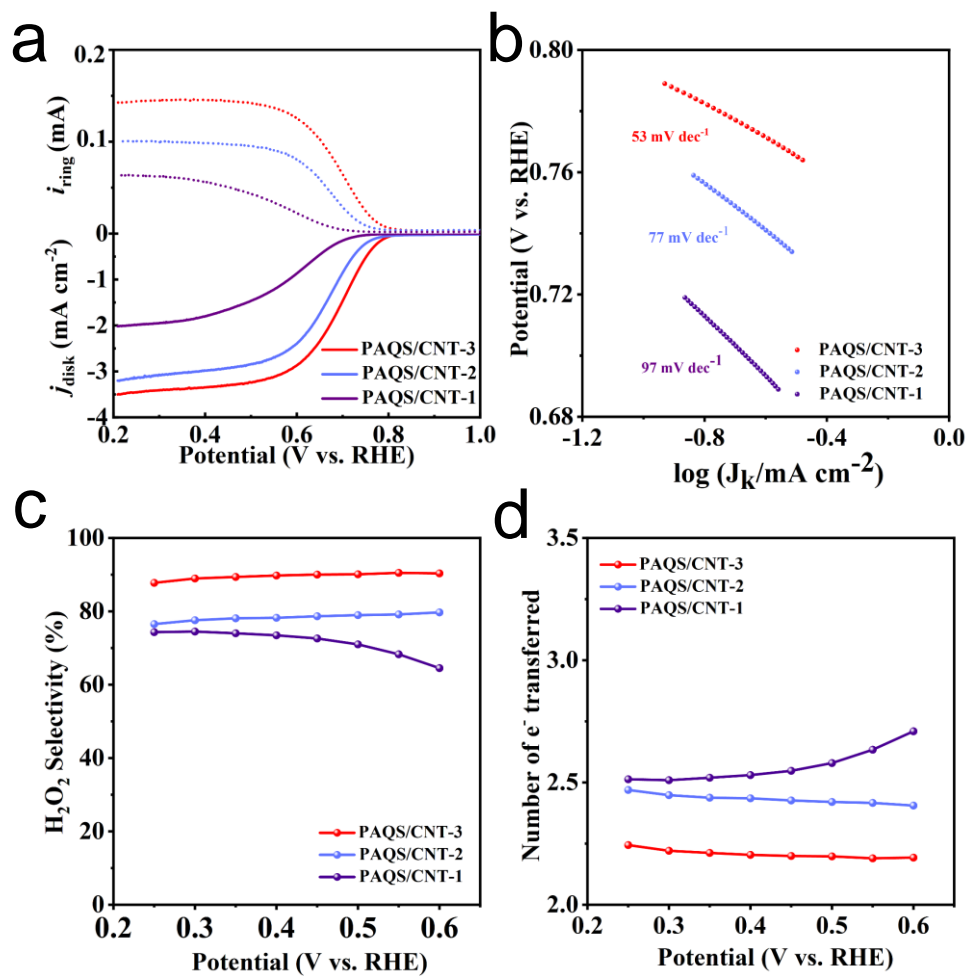


Figure S13. (a) RRDE voltammograms of PAQS/CNT-1, PAQS/CNT-2 and PAQS/CNT-3 for ORR and H_2O_2 production. (b) Tafel. (c) Number of transferred electrons. (d) Calculated selectivity.

Table S1. Electrocatalytic ORR performance comparisons of PAQS/CNT-3 with previously reported high-performance catalysts

Catalyst	Onset potential	Diffusion-limited current	Selectivity	Ref.
PAQS/CNT-3	0.78 V	3.5 mA cm⁻²	91%	This work
Co-N/O-C-0.9wt%C	0.75 V	2.5 mA cm ⁻²	95%	S1
CoOx/Co@CN _{y,700}	0.87 V	2.68 mA cm ⁻²	94.3%	S2
Mo-CDC-30	0.74 V	2.41 mA cm ⁻²	89.4%	S3
Ni _{2-x} P-VNi	0.78 V	2.96 mA cm ⁻²	>95%	S4
1% Co-SG	0.80 V	/	90%	S5
Ni ₃ B	0.70V	/	90%	S6
Mn-TiO ₂	0.78 V	/	92.7%	S7
BNT0	0.71 V	/	95%	S8

Reference

- S1. Y. Zheng, P. Wang, W. Huang, C. Chen, Y. Jia, S. Dai, T. Li, Y. Zhao, Y. Qiu, G. I. N. Waterhouse, G. Chen *Nano Lett.* 2023, **23**, 1100-1108
- S2. S. Zhang, S. Li, J. Liu, L. Kan, F. Rong, L. He, Z. Zhang, *Journal of Colloid and Interface Science*, 2023, **631**, 101-113
- S3. C. Zhang, C. Wu, L. Wang, G. Liu, *ACS Appl. Mater. Interfaces.*, 2023, **15**, 838-847
- S4. Z. Zhou, Y. Kong, H. Tan, Q. Huang, C. Wang, Z. Pei, H. Wang, Y. Liu, Y. Wang, S. Li, X. Liao, W. Yan, S. Zhao. *Adv. Mater.* 2022, **34**, 2106541
- S5. N Li, X Song, L Wang, X Geng, H Wang, H Tang, Z Bian, *ACS Appl. Mater. Interfaces* 2020, **12**, 24019-24029
- S6. F. Ma, S. Wang, X. Liang, C. Wang, F. Tong, Z. Wang, P. Wang, Y. Liu, Y. Dai, Z. Zheng, B. Huang. *Appl. Catal. B: Environ.*, 2020, **279**, 119371
- S7. Q. Chen, C. Ma, S. Yan, J. Liang, K. Dong, Y. Luo, Q. Liu, T. Li, Y. Wang, L. Yue, B. Zheng, Y. Liu, S. Gao, Z. Jiang, W. Li, X. Sun. *ACS Appl. Mater. Interfaces* 2021, **13**, 46659-46664
- S8. Z. Zhang, Q. Dong, P. Li, S. L. Fereja, J. Guo, Z. Fang, X. Zhang, K. Liu, Z. Chen, W. Chen. *J. Phys. Chem. C* 2021, **125**, 24814-24822